

Article

Investigating the Crystallization Process of Boron-Bearing Silicate-Phosphate Glasses by Thermal and Spectroscopic Methods

Magdalena Szumera ^{1,*} , Barbara Łagowska ¹, Justyna Sułowska ¹ , Piotr Jeleń ¹ , Zbigniew Olejniczak ² , Radosław Lach ¹, Anna Berezicka ¹ and Agnieszka Kijo-Kleczkowska ³

¹ Faculty of Materials Science and Ceramics, AGH University of Science and Technology, A. Mickiewicza 30, 30-059 Krakow, Poland; lagowska@agh.edu.pl (B.Ł.); sulowska@agh.edu.pl (J.S.); pjelen@agh.edu.pl (P.J.); Radoslaw.Lach@agh.edu.pl (R.L.); berezicka@agh.edu.pl (A.B.)

² The Henryk Niewodniczanski Institute of Nuclear Physics, Polish Academy of Science, Radzikowskiego 152, 31-342 Krakow, Poland; zbigniew.olejniczak@ifj.edu.pl

³ Faculty of Mechanical Engineering and Computer Science, Czestochowa University of Technology, Armii Krajowej 21, 42-201 Czestochowa, Poland; a.kijo-kleczkowska@pcz.pl

* Correspondence: mszumera@agh.edu.pl; Tel.: +48-126-172-483

Abstract: Glasses and devitrificates from the $\text{SiO}_2\text{-B}_2\text{O}_3\text{-P}_2\text{O}_5\text{-K}_2\text{O-CaO-MgO}$ system with constant contents of SiO_2 and P_2O_5 network formers, modified by the addition of B_2O_3 , were analyzed. All materials were synthesized by the traditional melt-quenching technique. The glass stability (GS) parameters (K_{rg} , ΔT , K_{W} , K_{H}) were determined. The effect of the addition of B_2O_3 on the GS, liquation phenomenon, crystallization process, and the type of crystallizing phases were examined using SEM-EDS, DSC, XRD, and Raman spectroscopy imaging methods. It was observed that the addition of B_2O_3 increased the tendency of the glass to crystallize. Both phosphates (e.g., $\text{Ca}_9\text{MgK}(\text{PO}_4)_7$, $\text{Mg}_3\text{Ca}_3(\text{PO}_4)_4$), and silicates (e.g., $\text{K}_2\text{Mg}_5(\text{Si}_{12}\text{O}_{30})$, $\text{CaMg}(\text{Si}_2\text{O}_6)$, MgSiO_3) crystallized in the studied system. The Raman spectrum for the orthophosphate $\text{Mg}_3\text{Ca}_3(\text{PO}_4)_4$ stanfieldite type was obtained. Boron ions were introduced into the structures of crystalline compounds at high crystallization temperatures. The type of crystallizing phases was found to be related to the phenomenon of liquation, and the order of their occurrence was dependent on the Gibbs free enthalpy.

Keywords: silicate–phosphate glasses; devitrificates; phase separation; crystallization; structure



Citation: Szumera, M.; Łagowska, B.; Sułowska, J.; Jeleń, P.; Olejniczak, Z.; Lach, R.; Berezicka, A.; Kijo-Kleczkowska, A. Investigating the Crystallization Process of Boron-Bearing Silicate-Phosphate Glasses by Thermal and Spectroscopic Methods. *Molecules* **2022**, *27*, 867. <https://doi.org/10.3390/molecules27030867>

Academic Editors: Qinghua Qin, Raj Das and Wugui Jiang

Received: 30 December 2021

Accepted: 22 January 2022

Published: 27 January 2022

Publisher's Note: MDPI stays neutral with regard to jurisdictional claims in published maps and institutional affiliations.



Copyright: © 2022 by the authors. Licensee MDPI, Basel, Switzerland. This article is an open access article distributed under the terms and conditions of the Creative Commons Attribution (CC BY) license (<https://creativecommons.org/licenses/by/4.0/>).

1. Introduction

It is known that crystallization processes, such as the crystallization of a glass, consist of three fundamental steps: the attainment of metastability, the formation of nuclei, and crystal growth [1]. When a liquid is cooled below its melting point, crystal nucleation can occur homogeneously or heterogeneously in the body of the liquid or on the surface. A typical glass-forming silicate melt is unique among solutions due to its ability to dissolve nearly all chemical elements. Such a melt is, therefore, a solution of oxides present in a thermodynamic equilibrium. Another unusual property of a glass-forming melt is its enormous change in viscosity with temperature. The viscosity of the material increases with cooling, but at certain temperatures, the mobility of molecules may still be great enough for a crystalline phase to form [2].

Liquation is considered a precrystallization ordering process [3]. Glasslike regions may form with the composition of the future crystals without simultaneous crystallization of these regions. Therefore, crystallization is preceded by a certain independent effect of primary precrystallizational demixing accompanied by a gain in thermodynamic potential. Separation of the precrystallizational phase (demixing) occurs by way of forming critically sized amorphous nuclei that are capable of further growth [4]. Precrystallization microphase separation is analogous to the usual metastable phase separation of the liquid

type, except that, first, in usual liquid metastable phase separation, the composition of the glasses deposited may differ greatly from the composition of the possible crystals and, second, it may appear and disappear reversibly without crystallization, depending on the temperature. Moreover, metastable phase separation occurs only in certain glasses in a definite composition region, whereas crystallization of glasses is possible with any composition and is irreversible below the solidus temperature. If metastable liquation were a purely precrystallization effect, it could not disappear with a rise in temperature once it had occurred, culminating in crystallization below the solidus [4]

The crystallization of multicomponent glasses consisting of two glass formers, i.e., SiO₂ and P₂O₅, SiO₂ and B₂O₂, or P₂O₅ and B₂O₃, is particularly complex. According to the literature, the crystallization process occurs in several stages, beginning with the formation of simple compounds built from chemical elements that are weakly bound to the glass structure and, therefore, are most mobile at a given temperature [5,6]. They play the role of nucleating agents. Compounds with more complex structures are formed in the next stages depending on the chemical composition of the glass.

In ternary system glasses, in which the matrix is formed by SiO₂ and B₂O₃ and one modifying component, the crystallization process generally has a single-stage or multi-stage character. The products of crystallization are usually borates (β -BaB₂O₄ [7], Ba₂Zn(BO₃)₂ [8], Mg₂B₂O₅ [9], CaB₂O₄ [10]) and silicates (Ba₅Si₈O₂₁ [7], BaZnSiO₄ [8], CaSiO₃, Ba₄Si₆O₁₆ [10]) in lower and higher temperature ranges, respectively. In the case of glasses containing P₂O₅ and B₂O₃ as matrix formers, the crystallization has a multistage character and the main products, at both lower and higher temperatures, are phosphates, e.g., Zn₂P₂O₇ [11], Li₃Fe₂(PO₄)₃, LiFeP₂O₇ [12], BaP₂O₅, BaBPO₅, and BPO₄ [11,13]. It is worth noting that the presence of boron ions in the structure of crystallizing phases is observed mainly at higher temperatures (above 590 °C) and at the minimum B₂O₃ content of 6 mol.% [11,13]. Lopes et al. [7] linked the type of crystallizing phase with the activation energy for crystallization. The authors of the publication concluded that the formation of the barium borate crystalline phase requires a lower activation energy, as it is generated in a loose borate-rich glass network structure, while the barium silicate crystalline phase has to be formed in a more interlocked silicate glass network structure. A similar approach to the study of glass crystallization was adopted by Kržmanc et al. [9], Liu [12], and Kalenda [13], while Zhu et al. [10] also considered the influence of the size of ions building the glass matrix on the type of crystallizing phase. Both Zhu et al. [10] and Hu et al. [14] agreed that the larger a cation's size, the lower its mobility, and thus the smaller the possibility of its occurrence in the crystallizing phases.

It is known that B₂O₃ is a strong glass networker; its presence in minor amounts possibly decreases the number of bridging oxygen atoms in silicate-based networks; thus, it may decrease the viscosity of the glass. Such behavior, which increases the mobility, is expected to promote devitrification at lower temperatures. This feature was exploited by Gou et al. [15], who modified 45Si5S glass (Hench glass) with B₂O₃ (0–6 mol.%) to decrease the heat treatment temperature of glass–ceramic analogues. The research shows that B₂O₃, apart from significantly decreasing the heat treatment of B₂O₃ containing 45S5 analogues, causes the desired phase of Na₂Ca₂Si₃O₉ to crystallize.

Fabert et al. [16] studied the partial to full substitution of SiO₂ with B₂O₃ in order to develop bioactive glasses with optimum thermal processing windows. Typical silicate bioactive glasses, such as S53P4 and 45S5, are known to be prone to crystallization upon heating. It has been shown that while borate glasses are unsuitable due to their limited hot forming domain, borosilicate glasses possess not only a wide hot forming domain but also a low activation energy for viscous flow. The crystallization rate of these borosilicate glasses was found to be lower than those of their borate and silicate counterparts.

In this work, we present a crystallization study of the multicomponent glasses from the SiO₂–B₂O₃–P₂O₅–K₂O–MgO–CaO system where the glass modifiers MgO and CaO are replaced in stages by B₂O₃. Such a study has not previously been reported in the literature. The studied materials have an interesting application as glassy fertilizers that introduce into

the soil environment, among others, boron and important microelements [17,18]. However, detailed knowledge of their structure and stability is required to optimize their properties. For this reason, the effects of the B₂O₃ content and glass modifiers, such as MgO, CaO, and K₂O, on the type of crystallizing phase was studied. The results of thermal tests were analyzed with structural studies (X-ray diffraction method) and microscopic observations (SEM-EDS analysis), including Raman spectroscopic imaging (RSI).

2. Materials and Methods

2.1. Synthesis of SiO₂–B₂O₃–P₂O₅–K₂O–CaO–MgO Glasses

Silicate–borate–phosphate glasses of SiO₂–B₂O₃–P₂O₅–K₂O–MgO–CaO composition were obtained by conventional melting of the respective chemically pure reagents (SiO₂, (NH₄)₂HPO₄, K₂CO₃, MgO, CaCO₃, and H₃BO₃) in platinum crucibles in the 1400–1450 °C temperature range. Glasses were quenched by immersing the crucibles in water. The choice of chemical composition of the tested glasses was based on previous studies of silicate–phosphate glasses used for agricultural applications [18,19]. The SiO₂ (41 mol.%), P₂O₅ (6 mol.%), and K₂O (6 mol.%) contents were kept constant in all glasses, whereas the amount of B₂O₃ (2–28 mol.%) increased at the cost of MgO and CaO, with the MgO/CaO ratio kept constant. The chemical composition of examined glasses is presented in Table 1. The amorphous character of the samples was confirmed by the X-ray diffraction method, which indicated that a fully amorphous material could only be obtained when the content of B₂O₃ did not exceed 25 mol.% [19].

Table 1. Nominal compositions of the analyzed glasses from the SiO₂–B₂O₃–P₂O₅–K₂O–MgO–CaO system [mol%].

Name of Sample	SiO ₂	P ₂ O ₅	B ₂ O ₃	K ₂ O	MgO	CaO	$\frac{B_2O_3}{B_2O_3+MgO+CaO}$
2B	41	6	2	6	27.0	18.0	0.042
4B	41	6	4	6	25.8	17.2	0.085
8B	41	6	8	6	23.4	15.6	0.170
10B	41	6	10	6	22.2	14.8	0.212
12B	41	6	12	6	21.0	14.0	0.255
14B	41	6	14	6	19.8	13.2	0.297
15B	41	6	15	6	19.2	12.8	0.319
20B	41	6	20	6	16.2	10.8	0.425
25B	41	6	25	6	13.2	8.8	0.531

2.2. Characterization

The FEI Nova NanoSEM 200 scanning electron microscope was used for SEM-EDS examinations of both glasses and their devitrificates. The observations were carried out under high vacuum conditions with a back scatter electron detector (BSE) and an accelerated voltage equal to 18 kV.

The thermal behavior of samples was studied with the STA 449 F3 Jupiter (NETZSCH) operating in DSC mode. Fifty milligram samples were ground to a grain size of 0.1–0.3 mm and placed in open Pt crucibles. The DSC measurements were carried out at a heating rate of 10 °C min^{−1} under the flowing air atmosphere (40 mL min^{−1}). Al₂O₃ was used as the reference material.

The glass stability (GS) [20] of studied glasses was determined by DSC analysis. The parameters describing the glass stability can be derived from the characteristic glass heating process temperatures T_g, T_x, T_c, and T_m, which correspond to the glass transition onset and the onset of and maximum crystallization peak, and the melting temperature, respectively. The most widely used are the Hruby [21], Weinberg [22], Lu and Liu [23], and Kosidis–Petrovic [20] parameters, which are defined by the following equations:

$$K_H = (T_x - T_g)/(T_m - T_x) \quad (1)$$

$$K_W = (T_c - T_g)/T_m \quad (2)$$

$$K_{rg} = T_g/T_m \quad (3)$$

Since the difference between T_x (or T_c) and T_g is another indicator of GS, it was also included in the analysis:

$$\Delta T = T_x - T_g \quad (4)$$

The DSC curves were evaluated with Proteus software (NETZSCH).

Once the crystallization temperatures of the selected samples were determined by DSC, the phase composition of the devitrificates was identified by XRD. For that purpose, the fraction containing the 0.1–0.3 mm particles was separated from the sample and heated isothermally for 12 h at the designated crystallization temperature. The phase compositions of the samples were identified via the X-ray diffraction analysis, based on the ICDD databases. XRD measurements were performed using a Empyrean diffractometer (Panalytical). The number of phases was determined through the Rietveld quantitative phase analysis using the High Score Plus software. The phase composition of the samples was quantified by Rietveld refinement and X-ray diffraction. X-ray diffraction patterns were obtained with a continuous scan. Empyrean (Malvern Panalytical) diffractometer fitted with a Cu tube operating at 45 kV, 30 mA was used to obtain data for the Rietveld refinement over the $5\text{--}90^\circ 2\theta$ with a step size of 0.08. The total measurement time was four hours. The content of the amorphous phase was found by applying the internal Al_2O_3 standard.

Raman imaging studies were carried out using a WITec Alpha 300 M+ spectrometer equipped with a 488 nm diode laser (laser spot was approx. 650 nm), 1800 grating, and a $100\times$ ZEISS Epiplan Neofluar objective. Imaging was conducted in a $20 \times 30 \mu\text{m}$ area and the scan parameters were as follows: 80 lines with 120 points per line and 120 lines with 80 points per line for the 2B and 20B samples, respectively. The single accumulation time was set to 1 s. All mathematical corrections were done using WITec Project Five 5.2 Plus software. In order to determine the chemical composition of the measured surface, a true component analysis was done. As a result, images as well as spectra of component distributions were obtained. The reference spectra were taken from the Horiba JY Raman Library (July 2008).

3. Results and Discussion

3.1. Characteristics of the Analyzed Glasses

Glasses containing B_2O_3 in their composition may demonstrate the phenomenon of phase separation. In the case of multi-component silicate–borate–phosphate glasses, it was determined that liquation in the examined system occurs when the B_2O_3 content is ≥ 8 mol.%. A further increase in B_2O_3 relative to the composition of the studied glasses, at the expense of MgO and CaO, intensifies this process until the glass is completely opaque. This phenomenon was confirmed by microscopic observations (Figures 1–3). The results of SEM-EDS observations showed that both separated phases contained components, i.e., silicon, phosphorus, potassium, magnesium, and calcium, introduced to the glass structure. However, it is worth noting that the semiquantitative EDS analysis showed different amounts of them in different areas of the examined samples. It turned out that one of the phases—later called phosphate—was enriched in P, Ca, and Mg (Figures 2b and 3b), while the other—later called silicate—contained increased amounts of Si and K (Figures 2a and 3a). This observation is crucial for the present study of the crystallization phenomenon, because it allowed the authors to demonstrate that the phenomenon of phase separation has a direct impact on the types of phases formed in the process of crystallization of their amorphous forms.

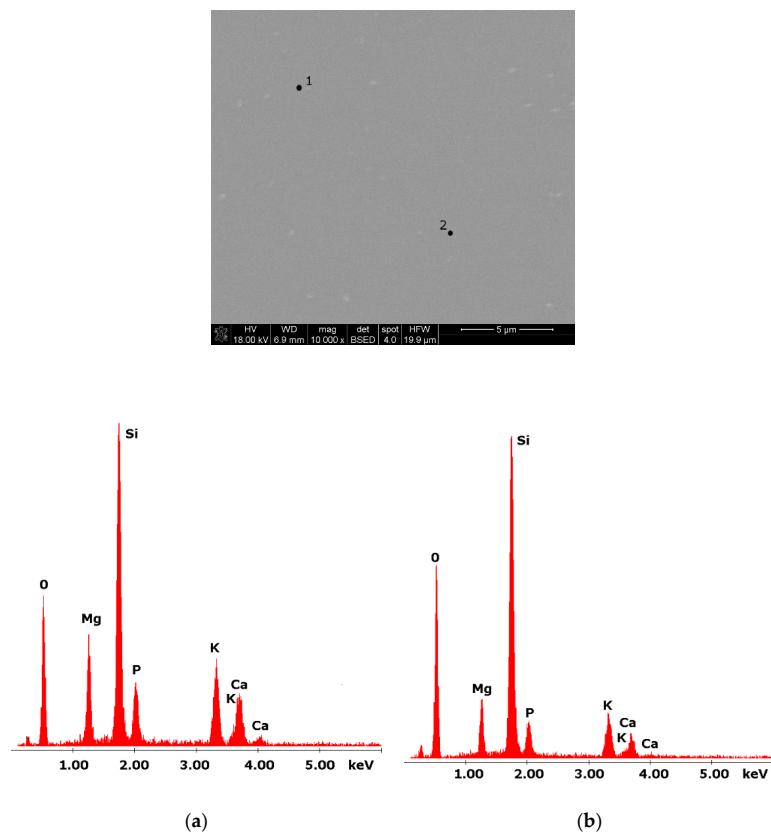


Figure 1. SEM microphotograph of 4B glass. (10,000×): (a) EDS analysis of 4B glass (p.1); (b) EDS analysis of 4B glass (p.2).

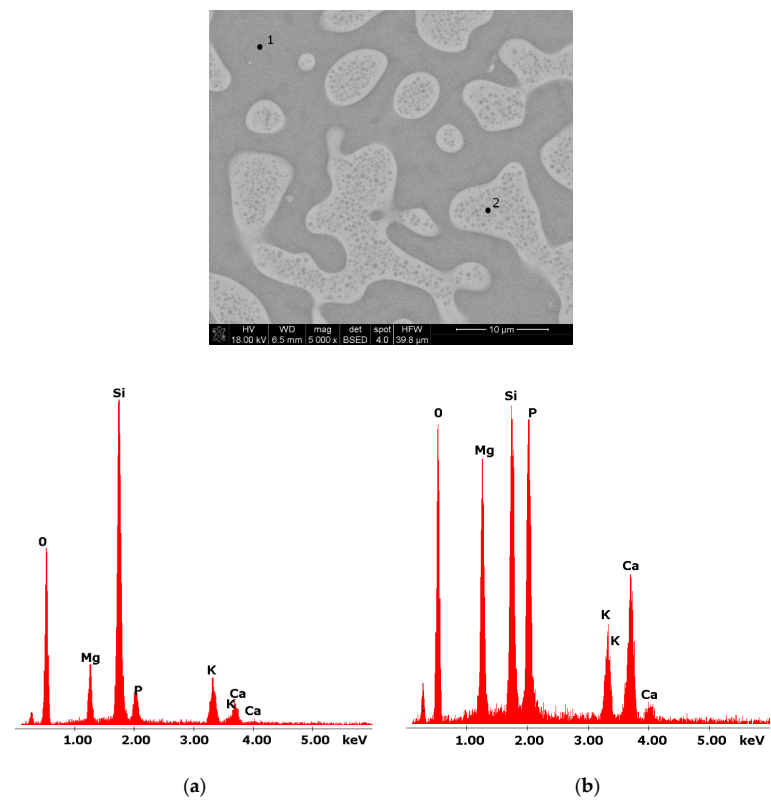


Figure 2. SEM microphotograph of 8B glass. (5000×) (a) EDS analysis of 8B glass (p.1); (b) EDS analysis of 8B glass (p.2).

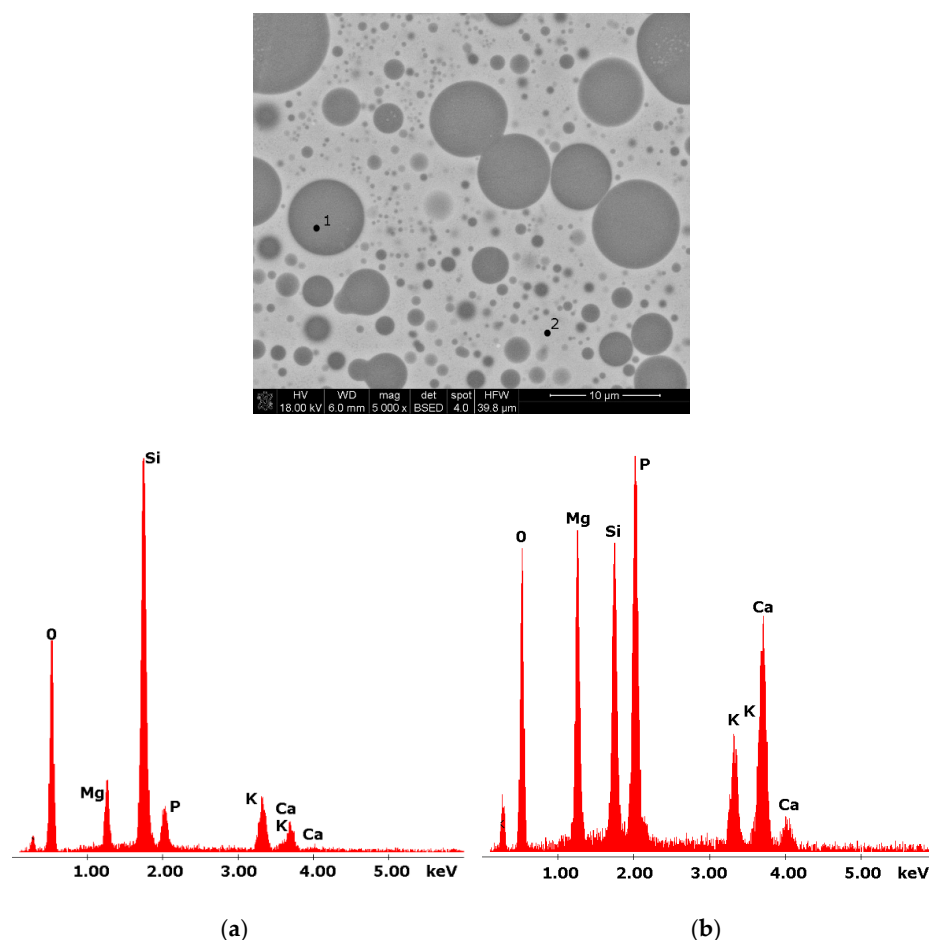


Figure 3. SEM microphotograph of 15B glass. (5000 \times) (a) EDS analysis of 15B glass (p.1); (b) EDS analysis of 15B glass (p.2).

3.2. Glass Stability vs. Phase Separation Phenomenon

The starting point for all of the presented studies was differential scanning calorimetry (DSC), which allowed us to observe transitions typical for the vitreous state, such as the glass transition (T_g range), crystallization (T_c range), and melting (T_m range). All obtained thermal curves are presented in Figure 4, and the values of selected thermal parameters determined from them (Section 2.2) are presented in Table 2. The thermal investigations conducted allowed us to determine the effect of increasing the amount of B_2O_3 introduced to the glass composition while diminishing the amounts of MgO and CaO on glass stability, the ability to crystallize, and the course, as well as to identify the types of crystallizing phases. On the basis of the obtained DSC curves, it was found that all of the studied glasses showed the ability to undergo multistage crystallization, the character of which depended on the $\frac{B_2O_3}{B_2O_3+MgO+CaO}$ ratio (Table 1).

At the lowest value of the above parameter (≤ 0.042), the crystallization had a two-stage character and occurred in the highest temperature ranges (above 800 $^{\circ}C$). As its value increased (≥ 0.085), the position of the first crystallization effect shifted towards lower temperatures and the character of the crystallization of the studied glasses changed from two-stage to three-stage. From that moment on, in the studied system, we were dealing with three-stage crystallization, which occurred until the value of $\frac{B_2O_3}{B_2O_3+MgO+CaO}$ exceeded 0.319. Then, the crystallization effect became a single, clearly visible, asymmetrical, exothermic effect.

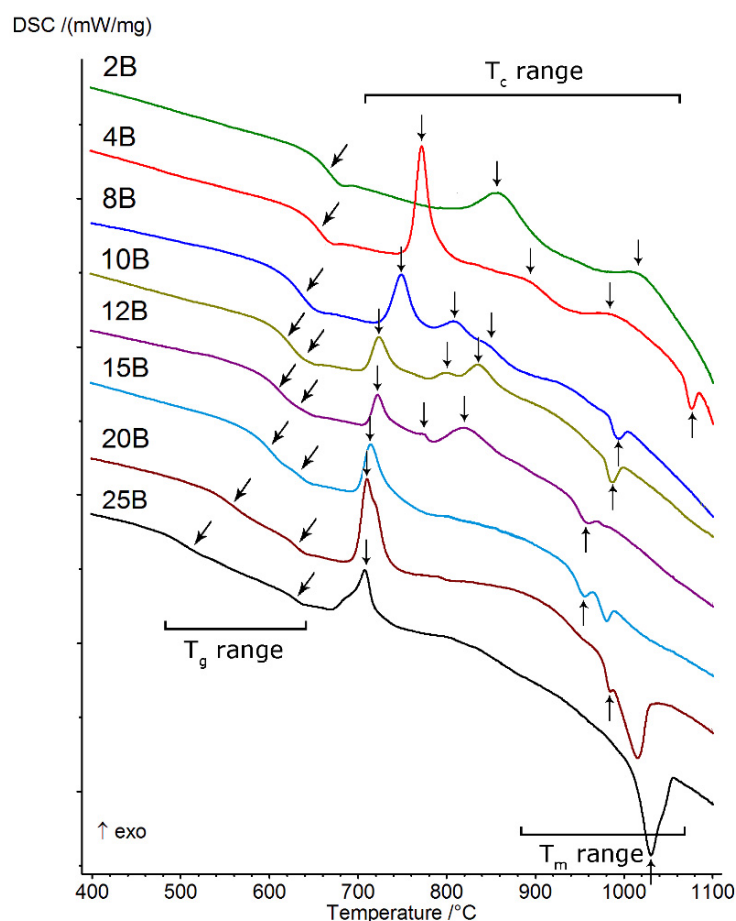


Figure 4. DSC curves of analyzed silicate–borate–phosphate glasses.

Table 2. Thermal characteristics of the analyzed glasses.

Sample	Glass Transition Range		Crystallization Range					Melting Range	The Glass Stability Parameters (GS)				
			Maximum Crystallization Peaks			Onset of Crystallization Peaks							
	$T_g/^\circ\text{C}$		$T_{c1}/^\circ\text{C}$	$T_{c2}/^\circ\text{C}$	$T_{c3}/^\circ\text{C}$	$T_{x1}/^\circ\text{C}$	$T_{x2}/^\circ\text{C}$	$T_{x3}/^\circ\text{C}$	$T_m/^\circ\text{C}$	$\Delta T/^\circ\text{C}$	K_W	K_H	K_{rg}
0B6P [24]	679		844	896		836			n.o.	157	n.o.	n.o.	n.o.
2B	660		858	1007		814	975		n.o.	154	n.o.	n.o.	n.o.
4B	651		772	886	988	756	858	952	1068	105	0.113	0.337	0.610
8B	631		749	808	847	726	785	829	983	95	0.120	0.370	0.642
10B	1st T_g	626	724			708			988	82	0.099	0.293	0.634
	2nd T_g	648	724	798	835	708	785	818	988	60	0.077	0.214	0.656
12B ⁸	1st T_g	614	722			708			958	94	0.113	0.376	0.641
	2nd T_g	642	722	775	819	708	n.o.	787	958	66	0.084	0.264	0.670
15B	1st T_g	606	714			699			956	93	0.113	0.362	0.634
	2nd T_g	634	714			699			956	65	0.084	0.253	0.663
20B	1st T_g	556	710			696			984	140	0.157	0.486	0.565
	2nd T_g	629	710	720 *		696			984	67	0.082	0.233	0.639
25B	1st T_g	502	708			672			1031	170	0.200	0.474	0.487
	2nd T_g	628	708	683 *		672			1031	44	0.078	0.123	0.609

* The inflection point of the exothermal effect.

The parameters determined from thermal curves (K_{rg} , ΔT , K_W , K_H), which prove the glass stability (GS) of the studied system, are also presented in Table 2. It was found that in the case of glasses that did not exhibit the phase separation phenomenon, for which $\frac{B_2O_3}{B_2O_3+MgO+CaO} \leq 0.170$, the ΔT parameter (as an indicator of GS) displayed gradually decreasing values, which indicates that the ability of the glasses to crystallize was gradually growing at the same time. In the case of liquation glasses ($\frac{B_2O_3}{B_2O_3+MgO+CaO} \geq 0.212$), for which a double effect of glass state transformation was successfully registered on DSC curves, two different tendencies related to their thermal stability were obtained. An analysis of the values indicated in Table 2 showed that, in the case of $\Delta T_{(1st)}$ ($\Delta T_{(1st)} = T_x - (1st)T_g$), the determined values gradually increased, while for $\Delta T_{(2nd)}$ ($\Delta T_{(2nd)} = T_x - (2nd)T_g$), they decreased. The direction of change in parameter $\Delta T_{(2nd)}$ was similar to that found for glasses that did not exhibit phase separation (2B, 4B, and 8B). It seems to the authors of the present study that this two-way behavior may signify that the thermal stability of the analyzed glasses depends, to some extent, on the transformation temperature T_g and the character of the separated phases, i.e., the amorphous silicate phase and phosphate phase, formed during the liquation process. This issue is discussed in detail in [24]. The determined for the ΔT parameter may prove that the amorphous phosphate phase, in comparison with the silicate phase, is associated with higher glass stability with respect to devitrification.

Furthermore, it is known that higher values for the K_{rg} , K_W , and K_H parameters (Table 2) imply greater resistance to the initiation of the amorphous phase of the crystallization process [2,5,25].

Therefore, the authors of the present study put forward the suggestion that the introduction of increasing amounts of B_2O_3 at the expense of MgO and CaO to the composition of glasses from the SiO_2 – B_2O_3 – P_2O_5 – K_2O – MgO – CaO system increases their tendency to undergo crystallization but also contributes to the decreased ease of glass formation.

3.3. Crystallization Process

To analyze the phenomenon of crystallization, it was necessary to subject the tested multi-component silicate–borate–phosphate glasses to an isothermal heating process, which was carried out in accordance with the procedure given in Section 2.2. This was related to their significant thermal stability (ΔT), presented in Table 2, and is discussed in more detail in Section 3.2.

The XRD analysis for the obtained devitrificates together with Rietveld refinement showed—despite many hours of heating samples—a relatively small degree of crystallization (Table 3). The amorphous phase represented 55% (for samples heated at higher temperatures, above 800 °C) to 72% (for samples heated in lower temperatures, below 800 °C).

3.3.1. X-ray Diffraction Analysis in the Study of Crystallization Products

The types of crystallization phases determined using the XRD method are shown in Table 3. XRD diffractograms of selected devitrificates are presented in Figures 5–7.

The obtained results clearly indicate the crystallization of two types of phase: complex phosphates and silicates. First of all, for $\frac{B_2O_3}{B_2O_3+MgO+CaO} < 0.212$, a single $Ca_9MgK(PO_4)_7$ -type whitlockite phosphate was crystallized. It is worth noting that this phase was also identified in the sample that was not modified with B_2O_3 [24]. However, when the value of $\frac{B_2O_3}{B_2O_3+MgO+CaO} \geq 0.212$ was reached, the phosphate phase $Mg_3Ca_3(PO_4)_4$ -type stanfieldite was a new product of crystallization in addition to the phosphate mentioned above. At the same time, by performing the Rietveld analysis, we managed to show that with an increase in the $\frac{B_2O_3}{B_2O_3+MgO+CaO}$ value, the share of the $Mg_3Ca_3(PO_4)_4$ phase gradually increased at the expense of the $Ca_9MgK(PO_4)_7$ phase. Its share increased from about 20% for $\frac{B_2O_3}{B_2O_3+MgO+CaO} = 0.212$ to about 72% for $\frac{B_2O_3}{B_2O_3+MgO+CaO} \geq 0.425$ and, finally, up to 100% for $\frac{B_2O_3}{B_2O_3+MgO+CaO} = 0.531$. The results of the XRD analysis showed that in higher

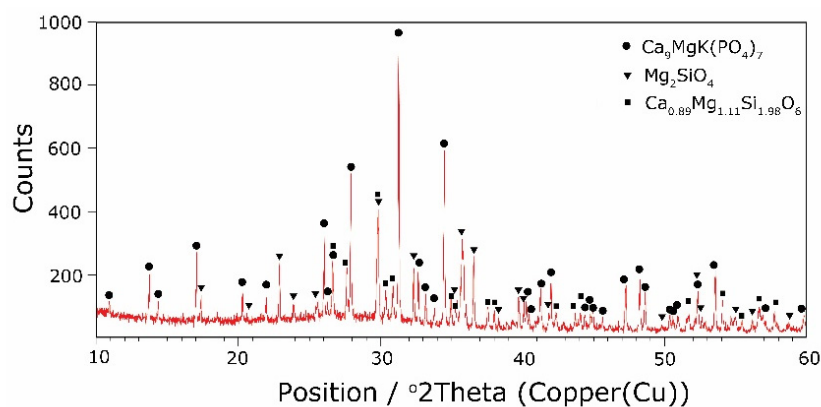
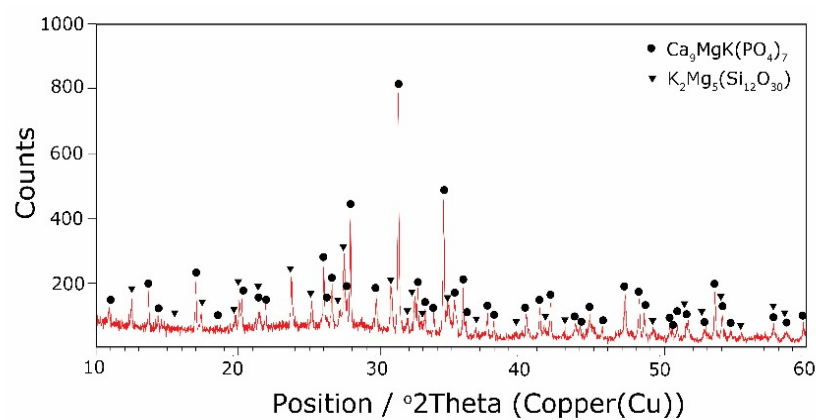
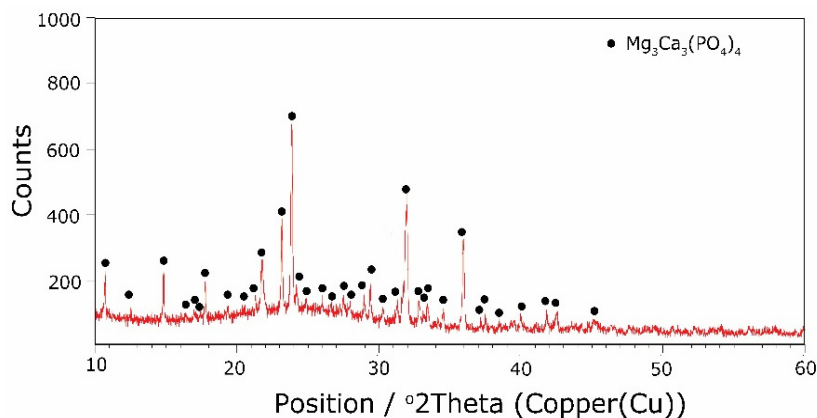
temperature ranges (above 800 °C), there were more crystallization products and these were more diversified, because apart from the phosphate phases, we also found the presence of silicate phases. Thus, at $\frac{B_2O_3}{B_2O_3+MgO+CaO} \leq 0.212$ in the temperature range from 800 to 910 °C, the presence of the $K_2Mg_5(Si_{12}O_{30})$ -merrihueite type silicate phase was confirmed next to $Ca_9MgK(PO_4)_7$. Rietveld's analysis confirmed that its share, regardless of the $\frac{B_2O_3}{B_2O_3+MgO+CaO}$ -ratio value, did not exceed 16%. In cases where crystallization effects were found at even higher temperatures—exceeding 980 °C—apart from permanently crystallizing phosphate (whitlockite type), silicates with a lower degree of polymerization, i.e., $MgSiO_3$ -enstatite type, Mg_2SiO_4 -forsterite type, and $CaMgSi_2O_6$ -diopside type were present.

Table 3. The kind of crystallizing phases identified in the analyzed devitrificates. Refined evaluation parameters used for the analysis are also reported.

No.	Crystallization Temperature (T _c) (°C)	Crystalline Phases	Reference Code	Fraction (%)	R _{wp}	P _p	χ ²
OB6P [18]	844	Ca ₉ MgK(PO ₄) ₇	n.o.				
	896	Ca ₉ MgK(PO ₄) ₇	n.o.				
2B	858	Ca ₉ MgK(PO ₄) ₇	98-008-5109	77.9	13.66	11.08	1.263
		K ₂ Mg ₅ (Si ₁₂ O ₃₀)	98-007-7131	21.1			
	1007	Ca ₉ MgK(PO ₄) ₇ Mg ₂ SiO ₄ CaMgSi ₂ O ₆	98-008-5109 98-020-2370 98-001-0224	80.5 17.1 2.4	10.79	9.4	0.854
4B	772	Ca ₉ MgK(PO ₄) ₇	98-008-5109	100	9.4	7.74	1.29
	886	Ca ₉ MgK(PO ₄) ₇	98-008-5109	79.9	12.94	10.17	1.223
		K ₂ Mg ₅ (Si ₁₂ O ₃₀)	98-007-7131	12.2			
		Ca _{9.5+0.5x} ((PO ₄) _{6-x} (BO ₃))(BO ₂) _{1-x} O _x	98-006-8336	7.9			
988	Ca ₉ MgK(PO ₄) ₇ MgSiO ₃ CaMg(Si ₂ O ₆) K(BSi ₂ O ₆)	98-008-5109 98-003-0893 98-008-9856 98-026-1715	79.9 15.8 3 1.3	10.49	8.84	0.72	
8B	749	Ca ₉ MgK(PO ₄) ₇	98-008-5109	100	10.73	9.39	0.629
	808	Ca ₉ MgK(PO ₄) ₇	98-008-5109	85	10.8	9.15	0.681
		K ₂ Mg ₅ (Si ₁₂ O ₃₀)	98-007-7131	15			
	847	Ca _{9.5+0.5x} ((PO ₄) _{6-x} (BO ₃))(BO ₂) _{1-x} O _x K(BSi ₂ O ₆)	98-008-5109 98-007-7131 98-006-8336 98-026-1715	81.8 7.5 8.4 2.3	10.1	8.4	0.747
10B	724	Ca ₉ MgK(PO ₄) ₇	98-008-5109	75.2	10.98	9.48	0.634
		Mg ₃ Ca ₃ (PO ₄) ₄	98-002-3642	24.8			
	798	Ca ₉ MgK(PO ₄) ₇	98-008-5109	84	10.77	9.12	0.606
		K ₂ Mg ₅ (Si ₁₂ O ₃₀)	98-007-7131	16			
835	Ca _{9.5+0.5x} ((PO ₄) _{6-x} (BO ₃))(BO ₂) _{1-x} O _x K(Bsi ₂ O ₆)	98-008-5109 98-007-2717 98-006-8336 98-026-1715	81.9 7.9 6.3 4	10.91	8.96	0.718	
12B	722	Ca ₉ MgK(PO ₄) ₇	98-008-5109	80.6	10.64	9.31	0.581
		Mg ₃ Ca ₃ (PO ₄) ₄	98-002-3642	19.4			
	819	Ca ₉ MgK(PO ₄) ₇ Mg ₃ Ca ₃ (PO ₄) ₄ K(Bsi ₃ O ₈)	98-008-5109 98-002-3642 98-006-9445	45.1 41.9 8.2	11.87	10.22	0.807
		Ca _{9.5+0.5x} ((PO ₄) _{6-x} (BO ₃))(BO ₂) _{1-x} O _x	98-006-8336	4.7			

Table 3. Cont.

No.	Crystallization Temperature (T_c) ($^{\circ}\text{C}$)	Crystalline Phases	Reference Code	Fraction (%)	R_{wp}	P_p	χ^2
15B	714	$\text{Ca}_9\text{MgK}(\text{PO}_4)_7$	98-008-5109	37.9	11.19	9.59	0.643
		$\text{Mg}_3\text{Ca}_3(\text{PO}_4)_4$	98-002-3642	62.1			
20B	710	$\text{Ca}_9\text{MgK}(\text{PO}_4)_7$	98-008-5109	8	14.04	11.9	0.931
25B	708	$\text{Mg}_3\text{Ca}_3(\text{PO}_4)_4$	98-002-3642	100	14.63	12.27	0.938

Figure 5. XRD patterns of 2B devitrificate obtained after isothermal heating at 1007 $^{\circ}\text{C}$ (no 2B_1007).Figure 6. XRD patterns of 10B devitrificate obtained after isothermal heating at 798 $^{\circ}\text{C}$ (no 10B_798).Figure 7. XRD patterns of 25B devitrificate obtained after isothermal heating at 708 $^{\circ}\text{C}$ (no 25B_708).

Next, the presence of boron ions in the resulting crystallization products was analyzed. Boron ions were found in both phosphates and silicates. The crystallizing phases were co-created generally in the higher temperature range (800–900 °C), which was at values of $0.085 \geq \frac{B_2O_3}{B_2O_3+MgO+CaO} \geq 0.252$. In the case of phosphates, the same non-stoichiometric compound, $Ca_{9.5+0.5x}((PO_4)_{6-x}(BO_3))(BO_2)_{1-x}O_x$, was always present. In the case of silicates, boron ions were initially present in the silicate $K(Bsi_2O_6)$, and then with an increase in the B_2O_3 content and decreases in MgO and CaO, its presence was found in the $K(Bsi_3O_8)$ silicate.

Considering the above, it is worth mentioning that the results for the type of crystallization phase are in accordance with the results of SEM-EDS analysis (Figures 2 and 3), which are mentioned in point 3.1. It is assumed that the observed phenomenon of liquation in the studied system affects the types of phases formed in the process of crystallization of their amorphous forms. On the basis of the SEM-EDS analysis, we found that the so-called phosphate phase was enriched with phosphorus, calcium, and magnesium (Figures 2b and 3b), while the silicate phase contained increased amounts of silicon and potassium or silicon, magnesium, and potassium (Figure 1a,b, 2a and 3a). Taking this into account and comparing the type of crystallizing phases (Table 3), we can see a significant convergence for the results obtained.

3.3.2. Spectroscopic Methods in the Study of Crystallization Products

The phase identification results (XRD analysis) were correlated with RSI (Raman spectroscopy imaging) studies. This method gave us the opportunity to generate detailed chemical images based on the Raman spectra of the sample (Figures 8–11). Two devitrificates, nos. 2B_1007 and 20B_710, were selected for the above analysis. They differed significantly in B_2O_3 content (Table 1) and phase crystallization type (Table 3). The Raman images obtained are presented in Figure 8, while the collected data from the designated areas are presented in Figure 9 for sample 2B_1007 and Figure 10 for sample 20B_710. Taking into account the information obtained from XRD studies, the identification process for the obtained spectra was related to the Raman spectra of standard substances. These spectra are presented in Figure 11 and they correspond to phosphate $Ca_9MgK(PO_4)_7$ and two silicates: Mg_2SiO_4 -forsterite type and $CaMgSi_2O_6$ -diopside type.

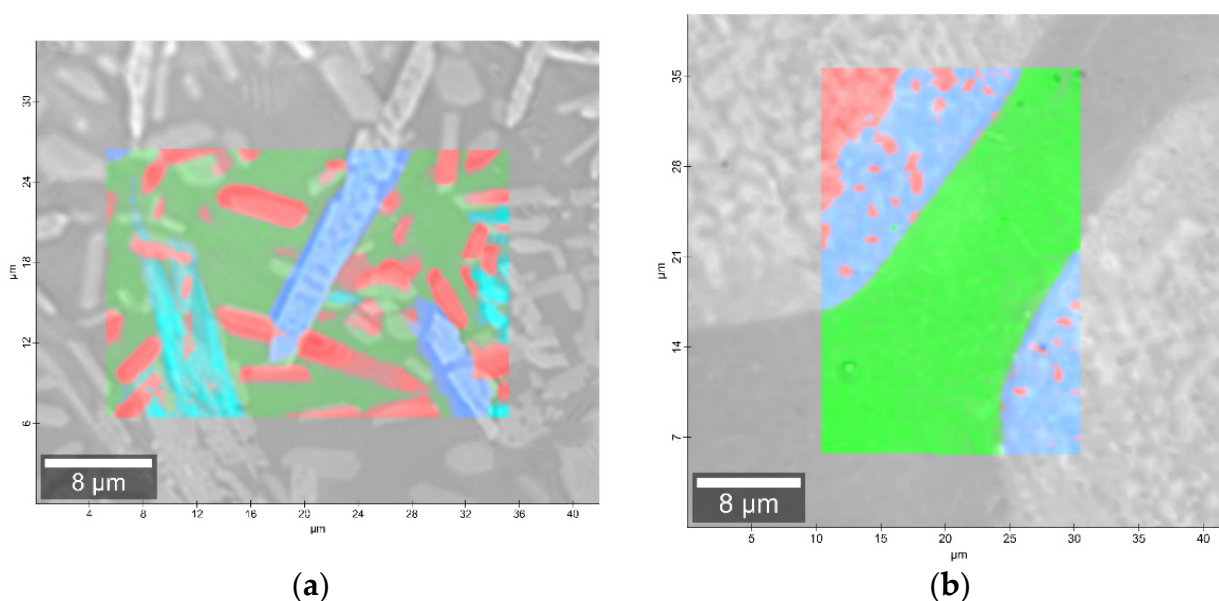


Figure 8. Microscopic images with overlaid Raman images of (a) 2B_1007 and (b) 20B_710 samples.

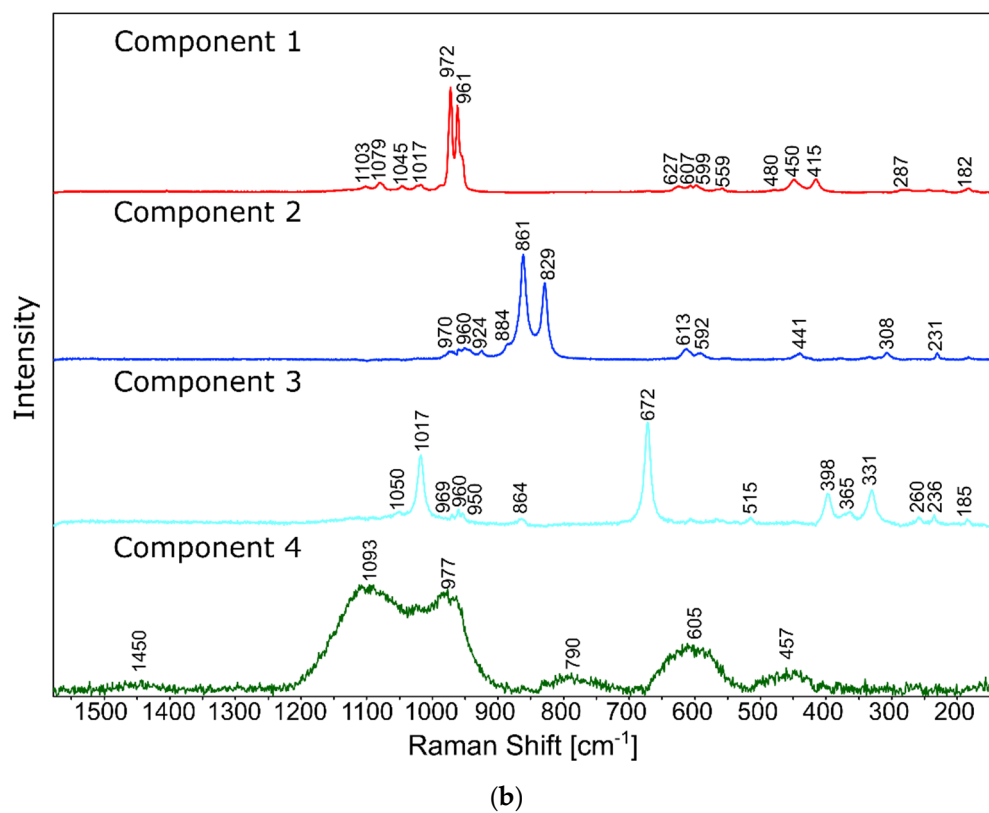
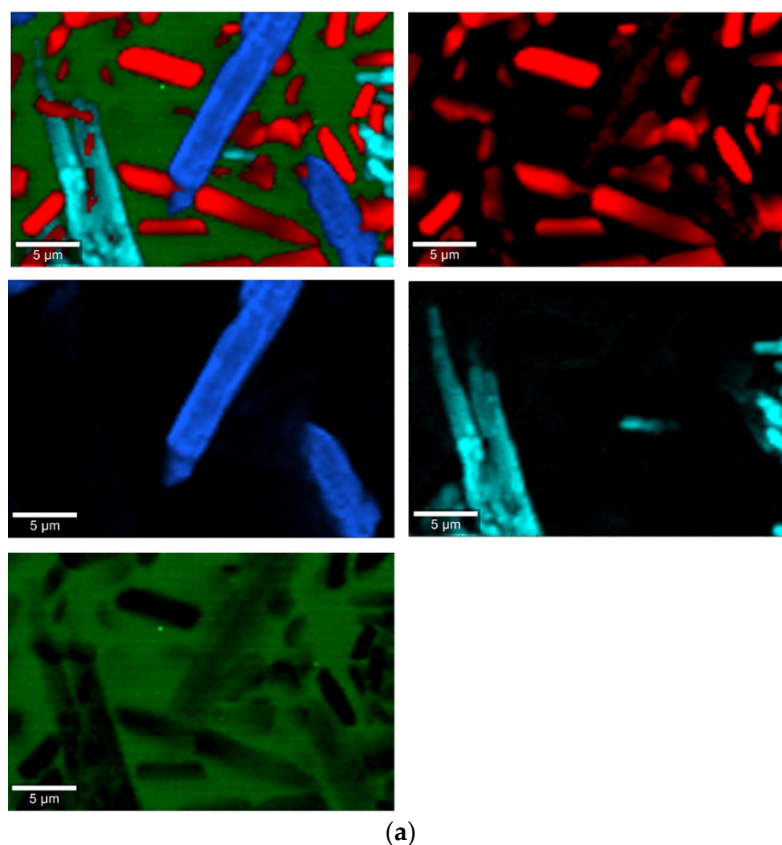
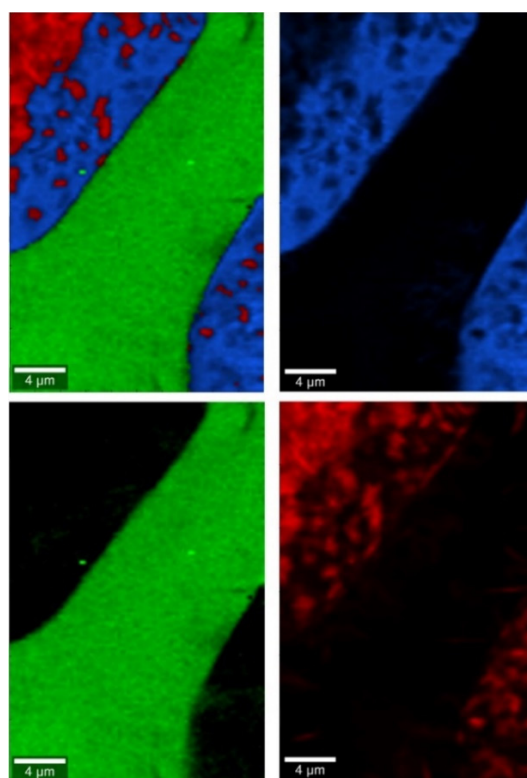
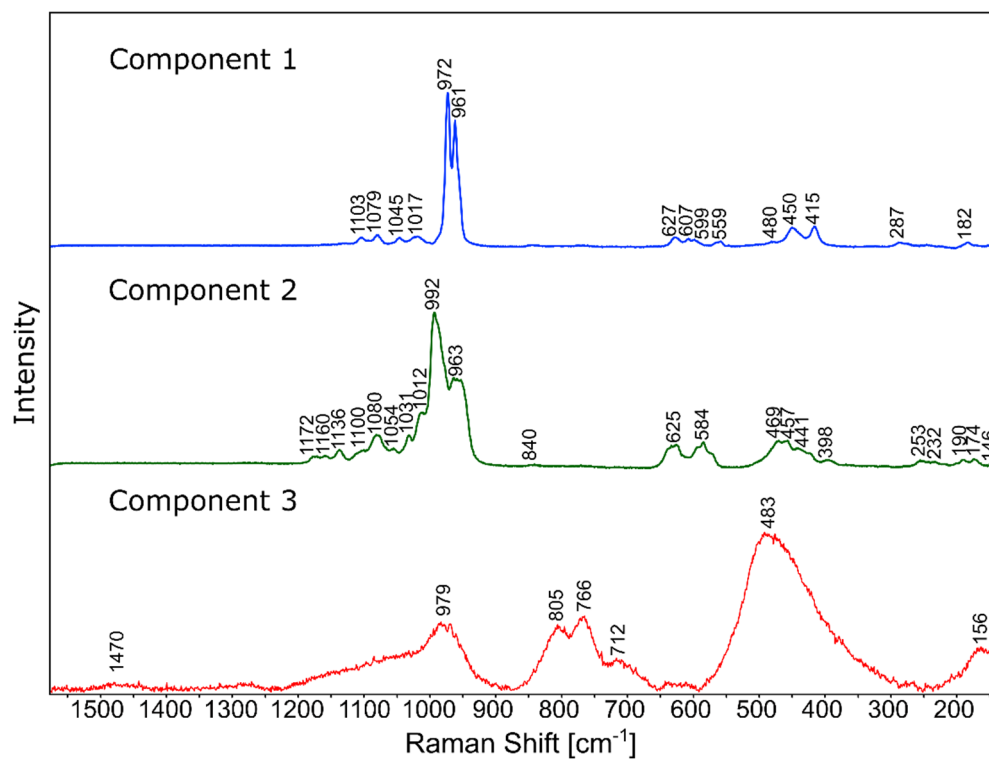


Figure 9. Raman measurements of sample 2B_1007. (a) Raman images obtained from the cluster analysis and (b) average Raman spectra from corresponding clusters: Component 1— $\text{Ca}_9\text{MgK}(\text{PO}_4)_7$ -whitlockite structure type, Component 2— Mg_2SiO_4 -forsterite type, Component 3— $\text{CaMgSi}_2\text{O}_6$ -diopside type, Component 4—glass matrix.



(a)



(b)

Figure 10. Raman measurements of sample 20B_710. (a) Raman images obtained from cluster analysis and (b) average Raman spectra from corresponding clusters: Component 1— $\text{Ca}_9\text{MgK}(\text{PO}_4)_7$ -whitlockite structure type, Component 2— $\text{Mg}_3\text{Ca}_3(\text{PO}_4)_4$ -stanfieldite type, Component 3—glass matrix.

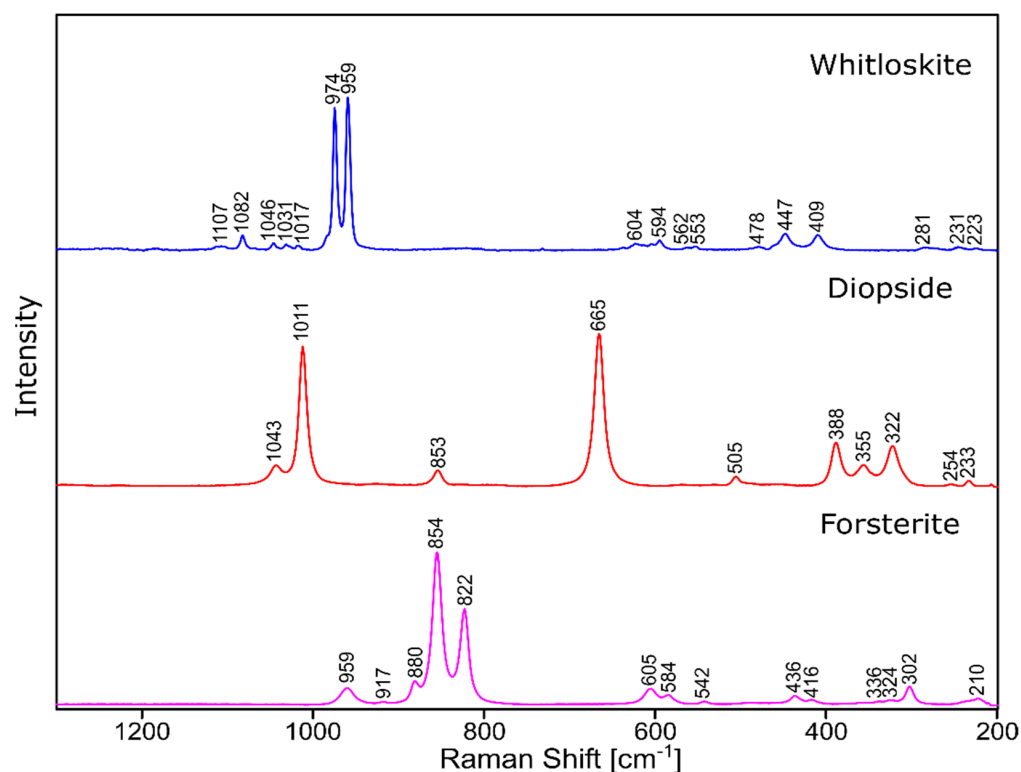


Figure 11. Raman spectra of standard substances.

In the case of the 20B_710 devitrificate, the situation is slightly more complicated. In this case, the glassy matrix (Component 3), marked in Figure 10 with red, was also visible. In this case, similarly to 2B_1007, the observed bands corresponded to the presence of structural units typical for a silicate–phosphate matrix, as described in [19], which also confirmed the presence of boron ions in the glassy matrix. It was demonstrated, among others, the presence of atoms in both triangular ($780\text{--}800$, $147\text{--}01470\text{ cm}^{-1}$) and tetrahedral ($760\text{--}770\text{ cm}^{-1}$) coordination as well as the formation of P–O–B ($600\text{--}640$, $1140\text{--}1150\text{ cm}^{-1}$) and B–O–Si ($\sim 480\text{ cm}^{-1}$) connections. At the same time, two further components of different structures—Component 1 (blue) and Component 2 (green)—were identified. Based on the Raman spectra obtained (Figure 10), Component 1 (blue) was identified as a phase with a complex phosphate $\text{Ca}_9\text{MgK}(\text{PO}_4)_7$ -whitlockite structure type. Unfortunately, the amount of published data on the Raman spectra of mineral phosphates is still limited, and we could not find a standard Raman spectrum for the phosphate $\text{Mg}_3\text{Ca}_3(\text{PO}_4)_4$ -stanfieldite type. However, taking into account our detailed and systematic XRD analysis of the series of devitrificates with a gradually changing chemical composition formed on the basis of glasses from the $\text{SiO}_2\text{--B}_2\text{O}_3\text{--P}_2\text{O}_5\text{--K}_2\text{O--MgO--CaO}$ system, it seems to be a reasonable proposal that Component’s 2 Raman spectrum (green), presented in Figure 10, comes from the phosphate $\text{Mg}_3\text{Ca}_3(\text{PO}_4)_4$ -stanfieldite type. Considering phosphate [26–29], it seems very likely that the green Raman spectra of phosphate oxyanions shows a symmetric stretching mode (ν_1) at about 992 and 963 cm^{-1} , the antisymmetric stretching mode (ν_3) at about 1012 and 1031 cm^{-1} , and the symmetric bending mode (ν_4) at about 625 and 584 cm^{-1} , while bands at about 470 to 398 cm^{-1} could be assigned to the ν_2 bending mode.

The results presented in Sections 3.3.1 and 3.3.2 are consistent and complement each other. They confirm that, depending on the temperature, boron ions either create or do not form crystalline phases and then remain in the vitreous matrix. Interestingly, the presence of boron ions in the vitreous matrix was not affected by the amount of B_2O_3 introduced into the glass composition but primarily by the crystallization temperature (T_c)—below or above $800\text{ }^\circ\text{C}$. Only in higher temperature ranges have boron ions been identified in both phosphates and silicates.

3.4. Chemical Affinity as a Factor Determining the Type of Crystallizing Phase

An attempt to explain the cause of crystallization of identified crystalline phases turned out to be of particular interest. For this purpose, we used the enthalpy values for the formation of phosphates and silicates from oxides (ΔG) at different temperatures [29], which are presented in Table 4.

Table 4. Values of ΔG for the formation of silicates and phosphates crystallizing in the analyzed glasses.

Compounds		ΔG [kJ/mol]		
		900 K	1000 K	1100 K
Ca ₉ MgK(PO ₄) ₇	9CaO·MgO·0.5K ₂ O·3.5P ₂ O ₅	−18,846.6	−19,196.9	−19,563.9
K ₂ Mg ₅ (Si ₁₂ O ₃₀)	K ₂ O·5 MgO·12 SiO ₂	−15,336.6	−15,534.0	−15,743.5
Mg ₃ Ca ₃ (PO ₄) ₄	3MgO·3CaO·2P ₂ O ₅	−10,716.1	−10,909.2	−11,111.5
CaMg(Si ₂ O ₆)	CaO·MgO·2SiO ₂	−3271.4	−3311.9	−3354.8
Mg ₂ SiO ₄	2MgO·SiO ₂	−2255.3	−2282.7	−2311.8
MgSiO ₃	MgO·SiO ₂	−1612.6	−1632.0	−1652.7

It was shown that, in this case, free enthalpy of crystallized compound formation is a factor that determines the type of crystallizing phases. It is known that the phase with the lowest negative ΔG value is the most likely to occur [29]. Thus, the crystallization of phosphates proceeds at the first stage of glass crystallization, while the crystallization of silicates occurs in the higher temperature range. This also applies to the phases containing boron ions. This also applies to the phases containing boron ions, case of which also first crystallize phosphates and then complex silicates (Table 5).

Table 5. Values of ΔG for the formation of silicates and phosphates containing boron crystallizing in the analyzed glasses.

Compounds		ΔG [kJ/mol]		
		900 K	1000 K	1100 K
Ca _{9.93} (P _{5.84} B _{0.16} O ₂₄)B _{0.67} O _{1.79}	9.93CaO·2.92 P ₂ O ₅ ·0.415B ₂ O ₃	−17,217.4	−17,526.0	−17,849.5
K(BSi ₂ O ₆)	0.5K ₂ O·0.5B ₂ O ₃ ·2SiO ₂	−2861.4	−2904.3	−2949.9
K(BSi ₃ O ₈)	0.5K ₂ O·0.5B ₂ O ₃ ·3SiO ₂	−3831.3	−3885.7	−3943.3

4. Conclusions

The main objective of this work was to study the influences of various B₂O₃ contents on the structure and crystallization processes of multicomponent glasses from the SiO₂–B₂O₃–P₂O₅–K₂O–MgO–CaO system. Complex multistage crystallization processes induced by the thermal treatment were characterized by SEM-EDS, DSC, XRD, and Raman spectroscopy mapping. It was found that the glass forming ability is limited to the amount of B₂O₃ (≤ 25 mol.%) present, and the phase separation phenomenon occurs with B₂O₃ ≥ 8 mol.%. Based on the obtained results, it was possible to link the phenomenon of liquation with the type of crystallizing phase. Simultaneously, it turned out that the increase in the content of B₂O₃ introduced while decreasing the contents of MgO and CaO in the silicate–phosphate network diminished the feasibility of undergoing glass formation and increased the ability of the glasses to crystallize. It was also found that the main phases crystallizing in the SiO₂–B₂O₃–P₂O₅–K₂O–CaO–MgO system were complex phosphates and silicates. The sequence of the appearance of crystallization products is governed by the free Gibbs enthalpy of phases formed from oxides; thus, phosphates first crystallize and then silicates. Boron ions appear in both types of crystalline phase but always at higher temperatures (above 800 °C); at lower temperatures, the phenomenon occurs in a vitreous network.

Author Contributions: Conceptualization, M.S. and B.Ł.; methodology, M.S. and J.S.; validation, M.S., Z.O., R.L. and P.J.; formal analysis, M.S. and A.B.; investigation, M.S.; data curation, M.S. and B.Ł.; writing—original draft preparation, M.S.; writing—review and editing, Z.O., A.K.-K. and J.S.; visualization, M.S., Z.O., R.L. and P.J.; funding acquisition, M.S. All authors have read and agreed to the published version of the manuscript.

Funding: This work was performed within the framework of funding for statutory activities of AGH University of Science and Technology in Krakow, Faculty of Materials Science and Ceramics (16.16.160.557). Research project partly supported by program “Excellence initiative—research university” for the AGH University of Science and Technology.

Institutional Review Board Statement: Not applicable.

Informed Consent Statement: Not applicable.

Data Availability Statement: Data available on request due to privacy restrictions. The data presented in this study are available on request from the corresponding author.

Acknowledgments: We thank Barbara Trybalska for SEM-EDS analysis.

Conflicts of Interest: The authors declare that they have no conflict of interest.

Sample Availability: Samples of the compounds are not available from the authors.

References

1. Duke, D.A. Glass: Theory of crystallization. In *Mineralogy. Encyclopedia of Earth Science*; Springer: Boston, MA, USA, 1981. [[CrossRef](#)]
2. Richardson, M.J. The Glass Transition Region. In *Calorimetry and Thermal Analysis of Polymers*; Method, V.B.F., Ed.; Hanser Publishers: Liberty Township, OH, USA, 1994; pp. 169–188.
3. Lebedeva, G.A. Formation of a Liquefaction structure in titanium-containing aluminosilicate glass. *Glass Ceram.* **2008**, *65*, 316–318. [[CrossRef](#)]
4. Uvarov, E.B. Catalyzed Crystallization of Glass. In *The Structure of Glass*; book series (SOG); Springer: Boston, MA, USA, 1964; Volume 3. [[CrossRef](#)]
5. Stoch, L. Thermochemistry of Solids with Flexible Structures. *J. Therm. Anal.* **1998**, *54*, 9–24. [[CrossRef](#)]
6. Stoch, L. Thermal analysis and thermochemistry of vitreous into crystalline state transition. *J. Therm. Anal. Cal.* **2004**, *77*, 7–16. [[CrossRef](#)]
7. Lopes, A.A.S.; Soares, R.S.; Lima, M.M.A.; Monteiro, R.C.C. Glass transition and crystallization kinetics of a barium borosilicate glass by a non-isothermal method. *J. App. Phys.* **2014**, *115*, 043516. [[CrossRef](#)]
8. Saisuk, Y.; Ayawanna, J.; Laorodphan, N. Crystallisation of BaO-ZnO-SiO₂-B₂O₃ Glasses: Effect of ZnO content, nucleation temperature and time. In Proceedings of the 34th MST Annual Conference, Bangkok, Thailand, 31 May–2 June 2017. [[CrossRef](#)]
9. Kržmanc, M.M.; Došler, U.; Suvorov, D. The nucleation and crystallization of MgO-B₂O₃-SiO₂ glass. *J. Eur. Ceram. Soc.* **2011**, *31*, 2211–2219. [[CrossRef](#)]
10. Zhua, H.; Fu, R.; Agathopoulos, S.; Fang, J.; Li, G.; He, Q. Crystallization behaviour and properties of BaO-CaO-B₂O₃-SiO₂ glasses and glass-ceramics for LTCC applications. *Ceram. Int.* **2018**, *44*, 10147–10153. [[CrossRef](#)]
11. Mošner, P.; Vosejpková, K.; Koudelka, L.; Benes, L. Thermal studies of ZnO-B₂O₃-P₂O₅-TeO₂ glasses. *J. Therm. Anal. Calorim.* **2012**, *107*, 1129–1135. [[CrossRef](#)]
12. Liu, S.; Yang, R.; Wang, Y. Effects of the substitution of P₂O₅ with B₂O₃ on the structure, iron valence, thermal and crystallization behavior of lithium-iron-phosphate glasses. *J. Non-Cryst. Solids* **2016**, *453*, 158–193. [[CrossRef](#)]
13. Kalenda, P.; Koudelka, L.; Mošner, P.; Benes, L. Thermal behavior and the properties of BaO-B₂O₃-P₂O₅ glasses. *J. Therm. Anal. Calorim.* **2016**, *124*, 1161–1168. [[CrossRef](#)]
14. Hu, Y.; Tsai, H.-T. The effect of BaO on the crystallization behaviour of a cordierite-type glass. *Mat. Chem. Phys.* **1998**, *52*, 184–188. [[CrossRef](#)]
15. Xie, K.; Zhang, L.; Yang, X.; Wang, X.; Yang, G.; Zhang, L.; Shao, H.; He, Y.; Fu, J.; Gou, Z. Preparation and Characterization of Low Temperature Heat-Treated 45S5 Bioactive Glass-Ceramic Analogues. *Biomed. Glasses* **2015**, *1*, 80–92. [[CrossRef](#)]
16. Fabert, M.; Ojha, N.; Erasmus, E.; Hannula, M.; Hokka, M.; Hyttinen, J.; Rocherulle, J.; Sigalasc, I.; Massera, J. Crystallization and sintering of borosilicate bioactive glasses for application in tissue engineering. *J. Mater. Chem. B* **2017**, *5*, 4514–4525. [[CrossRef](#)] [[PubMed](#)]
17. Waclawska, I.; Szumera, M. Reactivity of silicate-phosphate glasses in soil environment. *J. Alloy. Comp.* **2009**, *468*, 246–253. [[CrossRef](#)]
18. Szumera, M.; Waclawska, I.; Olejniczak, Z. Influence of B₂O₃ on the structure and crystallization of soil active glasses. *J. Therm. Anal. Cal.* **2010**, *99*, 879–886. [[CrossRef](#)]

19. Łagowska, B.; Waclawska, I.; Sitarz, M.; Szumera, M. Spectroscopic studies of structural interactions in silicate-boratephosphate glass. *J. Mol. Struct.* **2018**, *1171*, 110–116. [[CrossRef](#)]
20. Kozmidis-Petrovic, A.F. Theoretical analysis of relative changes of the Hruby, Weinberg, and Lu–Liu glass stability parameters with application on some oxide and chalcogenide glasses. *Thermochim. Acta* **2010**, *499*, 54–60. [[CrossRef](#)]
21. Hrubý, A. Evaluation of glass-forming tendency by means of DTA. *Czech. J. Phys. B* **1972**, *22*, 1187–1193. [[CrossRef](#)]
22. Weinberg, M.C. An assessment of glass stability criteria. *Phys. Chem. Glasses* **1994**, *35*, 119–123.
23. Lu, Z.P.; Liu, C.T. Glass Formation Criterion for Various Glass-Forming Systems. *Phys. Rev. Lett.* **2003**, *91*, 115505-1–115505-4. [[CrossRef](#)]
24. Łagowska, B.; Waclawska, I.; Sułowska, J.; Olejniczak, Z.; Sulikowski, B.; Szumera, M. Glass transition effect in liquation silicate–borate–phosphate glasses. *J. Therm. Anal. Calorim.* **2019**, *138*, 2251–2262. [[CrossRef](#)]
25. Vogel, W. Crystallization of Glasses. In *Glass Chemistry*; Vogel, W., Ed.; Springer: Berlin/Heidelberg, Germany, 1994; pp. 280–362. [[CrossRef](#)]
26. Brown, W.E.; Dickens, B. *Tschermaks Mineralogische und Petrographische Mitteilungen*, by Geologische Bundesanstalt (Austria). Jahrbuch. Supplement. SpringerLink (Online service). 1882, pp. 79–104. Available online: <https://hdl.handle.net/2027/nyp.33433069063000> (accessed on 22 December 2021).
27. Frost, L.R.; Wills, R.A.; Martens, W.N. A Raman spectroscopic study of synthetic giniite. *Spectrochim. Acta A* **2007**, *66*, 42–47. [[CrossRef](#)] [[PubMed](#)]
28. Lehr, J.R.; Brown, E.H.; Frazier, A.W.; Smith, J.P.; Thrasher, D. *Crystallographic Properties of Fertilizer Compounds*; Tennessee Valley Authority, National Fertilizer Development Center: Knoxville, TN, USA, 1967; p. 6. Available online: <https://books.google.pl/books?id=C9ikyAEACAAJ> (accessed on 22 December 2021).
29. Barin, I.; Knacke, O.; Kubaschewski, O. *Thermochemical Properties of Inorganic Substances*; Springer: Berlin/Heidelberg, Germany, 1973; ISBN 978-3-662-02293-1. [[CrossRef](#)]